

Status of next-generation $\Lambda_b \rightarrow p, \Lambda, \Lambda_c$ form-factor calculations

Stefan Meinel*

Department of Physics, University of Arizona, Tucson, AZ 85721, USA

E-mail: smeinel@arizona.edu

I present preliminary results of next-generation lattice-QCD calculations of the $\Lambda_b \rightarrow p$, $\Lambda_b \rightarrow \Lambda$, and $\Lambda_b \rightarrow \Lambda_c$ form factors based on RBC/UKQCD gauge-field ensembles with 2+1 flavors of domain-wall fermions. Compared to the work published in 2015 and 2016, the new calculations include three additional ensembles (one with 139 MeV pion mass, one with 0.073 fm lattice spacing, and one with another volume) and were performed with a more accurate tuning of the charm and bottom anisotropic clover action parameters.

*The 40th International Symposium on Lattice Field Theory (Lattice 2023)
July 31st - August 4th, 2023
Fermi National Accelerator Laboratory*

*Speaker

1. Introduction

Semileptonic decays of heavy baryons provide determinations of CKM matrix elements, constraints on flavor-changing neutral-current Wilson coefficients, and tests of lepton-flavor universality. The nonzero spins of the initial and final-state baryons make the decay amplitudes sensitive to all possible operator structures appearing in the weak effective Hamiltonian and allow a large number of angular observables that can be used to disentangle these structures. The most important charged-current bottom-baryon semileptonic decays are $\Lambda_b \rightarrow p\ell^-\bar{\nu}$ and $\Lambda_b \rightarrow \Lambda_c\ell^-\bar{\nu}$, which have been analyzed by LHCb to determine $|V_{ub}/V_{cb}|$ [1] and test τ -versus- μ lepton flavor universality [2]. The most important bottom-baryon FCNC decays are $\Lambda_b \rightarrow \Lambda\ell^+\ell^-$ and $\Lambda_b \rightarrow \Lambda\gamma$. LHCb measurements of the $\Lambda_b \rightarrow \Lambda\mu^+\mu^-$ differential branching fraction and $\Lambda_b \rightarrow \Lambda(\rightarrow p\pi^-)\mu^+\mu^-$ angular observables [3, 4] have been used to constrain the $b \rightarrow s\mu^+\mu^-$ Wilson coefficients $C_{9,10}^{(\prime)}$ [5].

The theoretical description of these decay processes involves hadronic matrix elements of the form $\langle F|\bar{q}\Gamma b|\Lambda_b\rangle$, where F is the baryon in the final state. These matrix elements can be expressed in terms of form factors f_0, f_+, f_\perp (for $\Gamma = \gamma^\mu$), g_0, g_+, g_\perp (for $\Gamma = \gamma^\mu\gamma_5$), and $h_+, h_\perp, \tilde{h}_+, \tilde{h}_\perp$ (for $\Gamma = \sigma_{\mu\nu}$) [6], which are functions of the four-momentum-transfer-squared, q^2 . The phenomenological applications cited above used lattice-QCD calculations of these form factors that were published in 2015 and 2016 [7, 8]. For the $|V_{ub}/V_{cb}|$ determination, the 2015 experimental and lattice uncertainties were about the same size, approximately 5% each [1, 7]. The LHCb measurement is projected to reach 2% precision with 50 fb^{-1} of integrated luminosity [9], requiring a commensurate improvement of the lattice-QCD calculation. For the $\Lambda_b \rightarrow \Lambda\mu^+\mu^-$ differential branching fraction at low q^2 , the 2015 experimental uncertainty [3] was already smaller than the uncertainty of the 2016 Standard-Model prediction using the form factors from lattice QCD [8], and in the meantime LHCb has accumulated much more data [10]. In summary, higher-precision lattice-QCD determinations of the $\Lambda_b \rightarrow p, \Lambda_b \rightarrow \Lambda, \text{ and } \Lambda_b \rightarrow \Lambda_c$ form factors are needed. I will report here on work underway toward this goal.

2. Parameters of the next-generation calculations

The ongoing next-generation calculations of the $\Lambda_b \rightarrow p, \Lambda, \Lambda_c$ form factors use the same types of lattice actions as the 2015/2016 calculations: the Iwasaki action for the gluons, domain-wall actions for the u, d , and s quarks, and anisotropic clover actions for the b and c quarks. The new calculations include three additional ensembles gauge-field configurations generated by the RBC and UKQCD collaborations [11, 12] and incorporate several other improvements as discussed in the following.

For reference, the upper part of Table 1 shows the data sets used in the 2015/2016 calculations. These data sets in fact come from three independent ensembles only. Partial quenching with $m_{u,d}^{(\text{val})} < m_{u,d}^{(\text{sea})}$ (highlighted in red color in the table) was used to generate the C14, C24, and F23 data sets to reach lower valence pion masses. This choice, however, resulted in small values of $m_\pi^{(\text{val})}L$ that made finite-volume errors the dominant systematic uncertainty in the ratio of decay rates relevant for the $|V_{ub}/V_{cb}|$ determination [7]. The data sets used for the next-generation calculations are shown in the lower part of Table 1. All six data sets now come from different ensembles and

Label	$N_s^3 \times N_t$	β	$am_{u,d}^{(\text{sea})}$	$am_{u,d}^{(\text{val})}$	$am_s^{(\text{sea})}$	$am_s^{(\text{val})}$	a [fm]	$m_\pi^{(\text{sea})}$ [MeV]	$m_\pi^{(\text{val})}$ [MeV]	Samples
C14	$24^3 \times 64$	2.13	0.005	0.001	0.04	0.04	≈ 0.111	≈ 340	≈ 250	2672
C24	$24^3 \times 64$	2.13	0.005	0.002	0.04	0.04	≈ 0.111	≈ 340	≈ 270	2676
C54	$24^3 \times 64$	2.13	0.005	0.005	0.04	0.04	≈ 0.111	≈ 340	≈ 340	2782
C53	$24^3 \times 64$	2.13	0.005	0.005	0.04	0.03	≈ 0.111	≈ 340	≈ 340	1205
F23	$32^3 \times 64$	2.25	0.004	0.002	0.03	0.03	≈ 0.083	≈ 304	≈ 230	1907
F43	$32^3 \times 64$	2.25	0.004	0.004	0.03	0.03	≈ 0.083	≈ 304	≈ 304	1917
F63	$32^3 \times 64$	2.25	0.006	0.006	0.03	0.03	≈ 0.083	≈ 361	≈ 361	2782

Label	$N_s^3 \times N_t$	β	$am_{u,d}^{(\text{sea,val})}$	$am_s^{(\text{sea})}$	$am_s^{(\text{val})}$	a [fm]	$m_\pi^{(\text{sea,val})}$ [MeV]	Samples
CP	$48^3 \times 96$	2.13	0.00078	0.0362	0.0362	≈ 0.114	≈ 139	80 ex, 2560 sl
C005LV	$32^3 \times 64$	2.13	0.005	0.04	0.0323	≈ 0.111	≈ 340	186 ex, 5022 sl
C005	$24^3 \times 64$	2.13	0.005	0.04	0.0323	≈ 0.111	≈ 340	311 ex, 4976 sl
F004	$32^3 \times 64$	2.25	0.004	0.03	0.0248	≈ 0.083	≈ 304	251 ex, 4016 sl
F006	$32^3 \times 64$	2.25	0.006	0.03	0.0248	≈ 0.083	≈ 361	223 ex, 3568 sl
F1M	$48^3 \times 96$	2.31	0.002144	0.02144	0.02217	≈ 0.073	≈ 232	113 ex, 3616 sl

Table 1: The data sets used for the 2015/2016 calculations [7, 8] (upper table) and for the ongoing next-generation calculations (lower table).

all use $m_{u,d}^{(\text{val})} = m_{u,d}^{(\text{sea})}$, satisfying $m_\pi L \gtrsim 4$. The CP ensemble has an approximately physical pion mass and the F1M ensemble has a third, finer lattice spacing; these two ensembles use a Möbius domain-wall action instead of the Shamir action used otherwise [11, 12]. The C005LV ensemble differs from C005 only in the lattice size. The valence strange-quark masses (highlighted in purple in the table where different from $m_s^{(\text{sea})}$) are now tuned to the physical values. I newly computed all quark propagators using all-mode averaging [13] with low-mode deflation for the light quarks; the numbers of exact and sloppy samples are annotated with “ex” an “sl” in the table. The Gaussian source smearing now uses APE-smearred gauge links, and the smearing width for the F004 and F006 data sets was increased compared to the 2015/2016 calculations to now match the width used on the C005/C005LV ensembles in physical units.

The actions used for the bottom and charm quarks have the form

$$S_Q = a^4 \sum_x \bar{Q} \left[m_Q + \gamma_0 \nabla_0 - \frac{a}{2} \nabla_0^{(2)} + \nu \sum_{i=1}^3 \left(\gamma_i \nabla_i - \frac{a}{2} \nabla_i^{(2)} \right) - c_E \frac{a}{2} \sum_{i=1}^3 \sigma_{0i} F_{0i} - c_B \frac{a}{4} \sum_{i,j=1}^3 \sigma_{ij} F_{ij} \right] Q. \quad (1)$$

By appropriately tuning the parameters am_Q , ν , c_E , and c_B for each lattice spacing, heavy-quark discretization errors that scale as powers of am_Q can be removed [14–19]. In the 2015/2016 Λ_b calculations, I used the bottom-quark parameters from Ref. [20]¹, which were tuned nonperturbatively using the $B_s^{(*)}$ dispersion relation and hyperfine splitting, and charm-quark parameters from Ref. [21], where the mass and anisotropy were tuned using the charmonium dispersion relation and c_E , c_B were set to the tadpole-improved tree-level values. For the second-generation Λ_b calculations, I performed a new tuning of the heavy-quark parameters, using updated lattice-spacing determinations from RBC/UKQCD [11, 12] and using the heavy-strange dispersion relation and hyperfine splitting for both bottom and charm. The B_s or D_s dispersion relation is

¹Reference [20] uses the notation $m_0 = m_Q$, $\zeta = \nu$ and $c_P = c_E = c_B$.

Ens.	am_Q	ν	$c_{E,B}$	aE_{B_s}	E_{B_s} [GeV]	$c_{B_s}^2$	$aE_{B_s^*} - aE_{B_s}$	$E_{B_s^*} - E_{B_s}$ [MeV]
CP	8.45	3.1	5.8	3.1084(13)	5.376(12)	0.914(13)	0.0288(13)	49.8(2.3)
CP	8.1476	3.3743	5.3944	3.1025(12)	5.366(12)	1.001(14)	0.0282(13)	48.8(2.3)
C005	7.42	2.92	4.86	3.00324(81)	5.360(15)	0.9184(89)	0.02602(52)	46.44(94)
C005	7.471	2.929	4.92	3.00801(81)	5.369(15)	0.9184(89)	0.02616(53)	46.69(95)
C005	7.9	2.929	4.92	3.05463(85)	5.452(15)	0.8895(91)	0.02482(53)	44.29(96)
C005	7.471	2.929	6	2.97872(77)	5.316(15)	0.9399(85)	0.03165(58)	56.5(1.1)
C005	7.471	3.3	4.92	3.03049(75)	5.409(15)	1.0186(89)	0.02665(48)	47.56(86)
C005	7.3258	3.1918	4.9625	3.00695(75)	5.367(15)	1.0013(88)	0.02719(49)	48.52(88)
F004	3.485	1.76	3.06	2.25010(82)	5.363(19)	0.855(12)	0.02053(62)	48.9(1.5)
F004	3.3	1.76	3.06	2.20958(79)	5.266(19)	0.877(12)	0.02148(61)	51.2(1.5)
F004	3.485	1.76	3.7	2.21551(78)	5.280(19)	0.877(12)	0.02468(68)	58.8(1.6)
F004	3.485	2.2	3.06	2.29690(70)	5.474(20)	1.047(12)	0.02126(51)	50.7(1.2)
F004	3.2823	2.0600	2.7960	2.25175(71)	5.366(19)	1.004(12)	0.02046(51)	48.8(1.2)
F1M	2.4538	1.7563	2.6522	1.97455(85)	5.347(20)	0.960(16)	0.01876(79)	50.8(2.2)
F1M	2.55	1.7563	2.6522	2.00012(88)	5.416(20)	0.943(17)	0.01821(81)	49.3(2.2)
F1M	2.4538	2	2.6522	2.00698(75)	5.435(20)	1.089(16)	0.01926(70)	52.2(1.9)
F1M	2.4538	1.7563	3.1	1.94472(81)	5.266(20)	0.983(16)	0.02151(83)	58.3(2.3)
F1M	2.3867	1.8323	2.4262	1.98009(81)	5.362(20)	1.003(16)	0.01799(73)	48.7(2.0)

Ens.	am_Q	ν	$c_{E,B}$	aE_{D_s}	E_{D_s} [GeV]	$c_{D_s}^2$	$aE_{D_s^*} - aE_{D_s}$	$E_{D_s^*} - E_{D_s}$ [MeV]
CP	0.14752	1.1928	1.7784	1.12144(43)	1.9395(43)	1.0075(52)	0.07903(59)	136.7(1.1)
CP	0.27077	1.1879	2.0714	1.13419(43)	1.9616(44)	1.0008(51)	0.08353(63)	144.5(1.1)
CP	0.27514	1.1883	2.0712	1.13804(43)	1.9682(44)	1.0000(51)	0.08317(63)	143.8(1.1)
C005	0.11360	1.2045	1.7936	1.08504(53)	1.9366(55)	1.0078(95)	0.08152(80)	145.5(1.5)
C005	0.11360	1.2045	1.72	1.10561(55)	1.9733(56)	1.0019(97)	0.07796(79)	139.1(1.5)
C005	0.11360	1.13	1.7936	1.04096(53)	1.8579(53)	0.9646(89)	0.08375(82)	149.5(1.5)
C005	0.14	1.2045	1.7936	1.10676(55)	1.9753(56)	1.0018(96)	0.07934(80)	141.6(1.5)
C005	0.15410	1.2004	1.8407	1.10274(54)	1.9682(56)	1.0001(95)	0.08057(81)	143.8(1.5)
F004	-0.01750	1.1039	1.5884	0.81570(39)	1.9441(71)	1.003(10)	0.06339(84)	151.1(2.1)
F004	-0.01750	1.1039	1.51	0.84109(41)	2.0046(73)	0.999(11)	0.05992(83)	142.8(2.0)
F004	-0.01750	1.05	1.5884	0.78075(39)	1.8608(68)	0.9674(99)	0.06513(85)	155.2(2.1)
F004	0.01	1.1039	1.5884	0.84309(40)	2.0093(73)	0.998(11)	0.06090(84)	145.1(2.1)
F004	-0.05167	1.1021	1.4483	0.82583(40)	1.9682(72)	1.000(11)	0.06032(82)	143.8(2.0)
F1M	-0.01508	1.0635	1.6094	0.72535(35)	1.9643(73)	0.9766(91)	0.05356(84)	145.0(2.3)
F1M	0.005	1.0635	1.6094	0.74696(38)	2.0228(75)	0.972(10)	0.05181(86)	140.3(2.4)
F1M	-0.01508	1.09	1.6094	0.74250(37)	2.0107(75)	0.994(10)	0.05274(84)	142.8(2.3)
F1M	-0.01508	1.0635	1.7	0.69066(29)	1.8703(69)	0.9844(80)	0.05757(82)	155.9(2.3)
F1M	-0.05874	1.0941	1.5345	0.72459(34)	1.9622(73)	1.0007(93)	0.05339(81)	144.6(2.3)

Table 2: Tuning of the bottom-quark action (upper table) and charm-quark action (lower table). Shown here are results obtained from fits to $B_s^{(*)}$ and $D_s^{(*)}$ two-point correlation functions for several choices of the action parameters, on four of the ensembles used. All energies listed here are at zero momentum. The final values of the action parameters, which satisfy the tuning conditions and were used for the new $\Lambda_b \rightarrow p, \Lambda, \Lambda_c$ form-factor calculations, are highlighted in green. The parameter choices highlighted in blue correspond to the central values of the bottom-quark parameters used by RBC/UKQCD [23]. The uncertainties on the bottom-quark parameters given in Ref. [23] are not propagated here.

written as $(aE(\mathbf{p}))^2 \approx (aM_{\text{rest}})^2 + c^2(a\mathbf{p})^2$, where $c^2 = M_{\text{rest}}/M_{\text{kin}}$. I calculated c^2 directly as $c^2 = [(aE(\mathbf{p}))^2 - (aE(\mathbf{0}))^2]/(a\mathbf{p})^2$ with $\mathbf{p}^2 = 1 \cdot (2\pi/L)^2$ and confirmed that higher momenta give consistent results. The tuning conditions are the same as in Ref. [20]: $E_{H_s}(\mathbf{0}) = M_{H_s, \text{exp}}$, $c_{H_s}^2 = 1$, and $E_{H_s^*}(\mathbf{0}) - E_{H_s}(\mathbf{0}) = M_{H_s^*, \text{exp}} - M_{H_s, \text{exp}}$, where the experimental values are taken from Ref. [22]. My results for these quantities for several choices of the heavy-quark parameters are shown in Table 2. The final choice for am_Q , ν , $c_E = c_B$ (highlighted in green) on each ensemble was obtained using a linear fit to the other results and solving the tuning conditions for the parameters. Runs with these final parameters then confirmed that the tuning conditions are indeed satisfied.

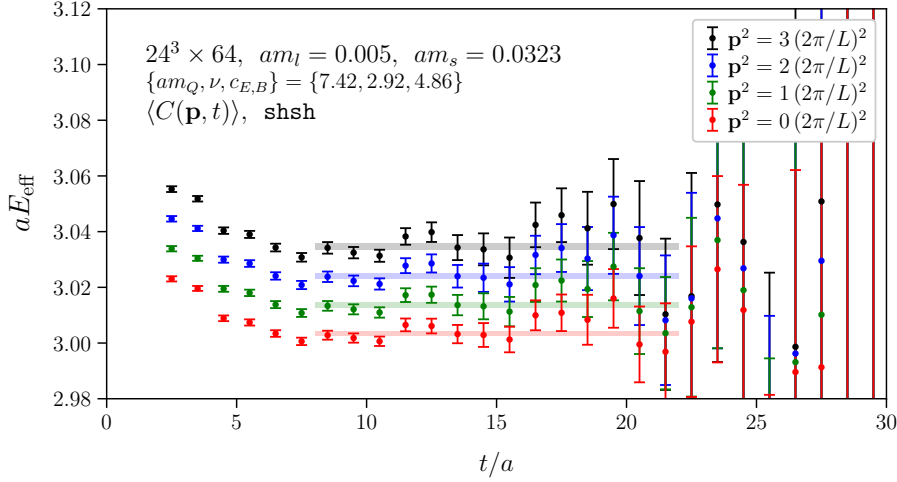


Figure 1: Effective energies of B_s two-point functions used for the tuning of the bottom-quark parameters.

Note that the RBC and UKQCD collaborations also updated their tuning [20] of the bottom-quark parameters using the new lattice-spacing determinations from Ref. [11] and shared their results with me; these new parameters have since been published in Ref. [23]. I tested the central values of the parameters determined by RBC/UKQCD, as shown in the columns highlighted in blue in Table 2. I found that, while the B_s energy at zero momentum and the hyperfine splitting agree with experiment, the c^2 values are 8% and 14% below 1 on the C005 and F004 ensembles, respectively (Ref. [23] also presents uncertainties on the heavy-quark parameters which I did not propagate here). In contrast, RBC/UKQCD obtained c^2 equal to 1. My proposed explanation for this discrepancy is the following. Due to the particular choice of smearing scheme in Ref. [20], the excited-state contamination in the two-point functions shows a strong momentum dependence, as can be seen in Fig. 4 of Ref. [20]. When computing the very small differences in $(aE)^2$ between zero and nonzero momentum, there is a large cancellation in statistical uncertainties due to correlations. However, the excited-state contamination in $(aE)^2$ changes sign from negative to positive as \mathbf{p}^2 is increased. Thus, the excited-state contamination in the energy difference or slope is *enhanced* and leads to an overestimate of c^2 . I used a different smearing scheme for which the excited-state contamination in the two-point functions is almost momentum-independent, as shown in Fig. 1.

The 2015/2016 calculations of the Λ_b -decay form factors used the “mostly nonperturbative” method [24, 25] to renormalize and $\mathcal{O}(a)$ -improve the weak currents. The renormalized and improved $b \rightarrow q$ currents ($q = u, s, c$) are of the form

$$J_\Gamma = \sqrt{Z_V^{qq} Z_V^{bb}} \rho_\Gamma \left[\bar{q} \Gamma b + \mathcal{O}(a) \text{ improvement terms} \right], \quad (2)$$

where Z_V^{bb} , Z_V^{qq} are the renormalization factors of $\bar{q}\gamma^0 q$ and $\bar{b}\gamma^0 b$, computed nonperturbatively using charge conservation, and the residual matching coefficients ρ_Γ as well as the $\mathcal{O}(a)$ improvement coefficients are computed to one loop in lattice perturbation theory [7] (tree-level only for the tensor currents). For the preliminary analysis of the next-generation form-factor data shown in the following, I use the same method. I newly computed Z_V^{bb} and Z_V^{cc} for the updated heavy-quark parameters from Table 2 using ratios of zero-momentum B_s/D_s two-point and three-point

Ensemble	Z_V^{ll}	Z_V^{cc}	Z_V^{bb}
CP	0.71076(25) [11]	1.40756(17)	9.9128(81)
C005, C005LV	0.71273(26) [11]	1.35761(16)	9.0631(84)
F004, F006	0.7440(18) [11]	1.160978(74)	4.7449(21)
F1M	0.761125(19) (Z_A , F1S) [26]	1.112316(61)	3.7777(23)

Table 3: My results for the nonperturbative renormalization factors Z_V^{cc} and Z_V^{bb} , along with the values I currently use for Z_V^{ll} ($l = u, s$). For the F1M ensemble, Z_V^{ll} was not yet available, so in this preliminary analysis I used the value Z_A^{ll} from the F1S ensemble [26] that differs from F1M only by having the Shamir domain-wall action instead of the Möbius action [12].

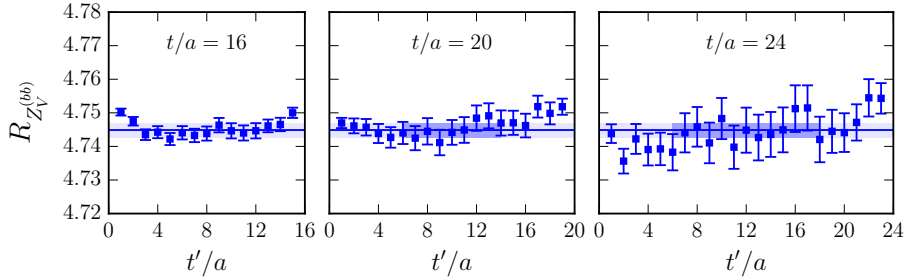


Figure 2: Numerical results for the ratio of zero-momentum B_s two-point and three-point functions (with the current $\bar{b}\gamma^0 b$) that gives Z_V^{bb} , from the F004 ensemble. Here, t is the source-sink separation and t' is the current insertion time. The dark-shaded regions are included in the constant fit.

functions. Example plots of these ratios are shown in Fig. 2. My results for Z_V^{cc} and Z_V^{bb} , along with the values I currently use for Z_V^{ll} ($l = u, s$), are given in Table 3. For the residual-matching and $O(a)$ -improvement coefficients in the preliminary analysis, I still use the values from Ref. [7], which were computed for the old heavy-quark-action parameters. For the CP ensemble, for now, I use the same values as for C005. For the F1M ensemble, I extrapolated the values from Ref. [7] linearly in the lattice spacing.

3. Preliminary form-factor results

The form factors are obtained from products of forward and backward $\Lambda_b \rightarrow F$ ($F = p, \Lambda, \Lambda_c$) three-point functions divided by a product of the Λ_b and F two-point functions; in these ratios, the overlap factors and time dependence cancel for the ground-state contribution [7]. The calculations are done in the Λ_b rest frame, for final-state momenta in the range $0 < |\mathbf{p}'| \lesssim 1.5$ GeV, and for all possible source-sink separations in the range $0.4 \text{ fm} \lesssim t \lesssim 1.7 \text{ fm}$. The ratio is evaluated at current-insertion time $t' = t/2$, where excited-state contamination is expected to be minimal. By multiplying with the appropriate kinematic factors and taking the square root, quantities $R_f(|\mathbf{p}'|, t)$ are obtained that are equal to the form factor $f(|\mathbf{p}'|)$ up to excited-state contamination that decays exponentially with t [7]. I have performed preliminary fits of the t dependence to extract the ground-state form factors, but I am still working on the estimates of the uncertainties. For this

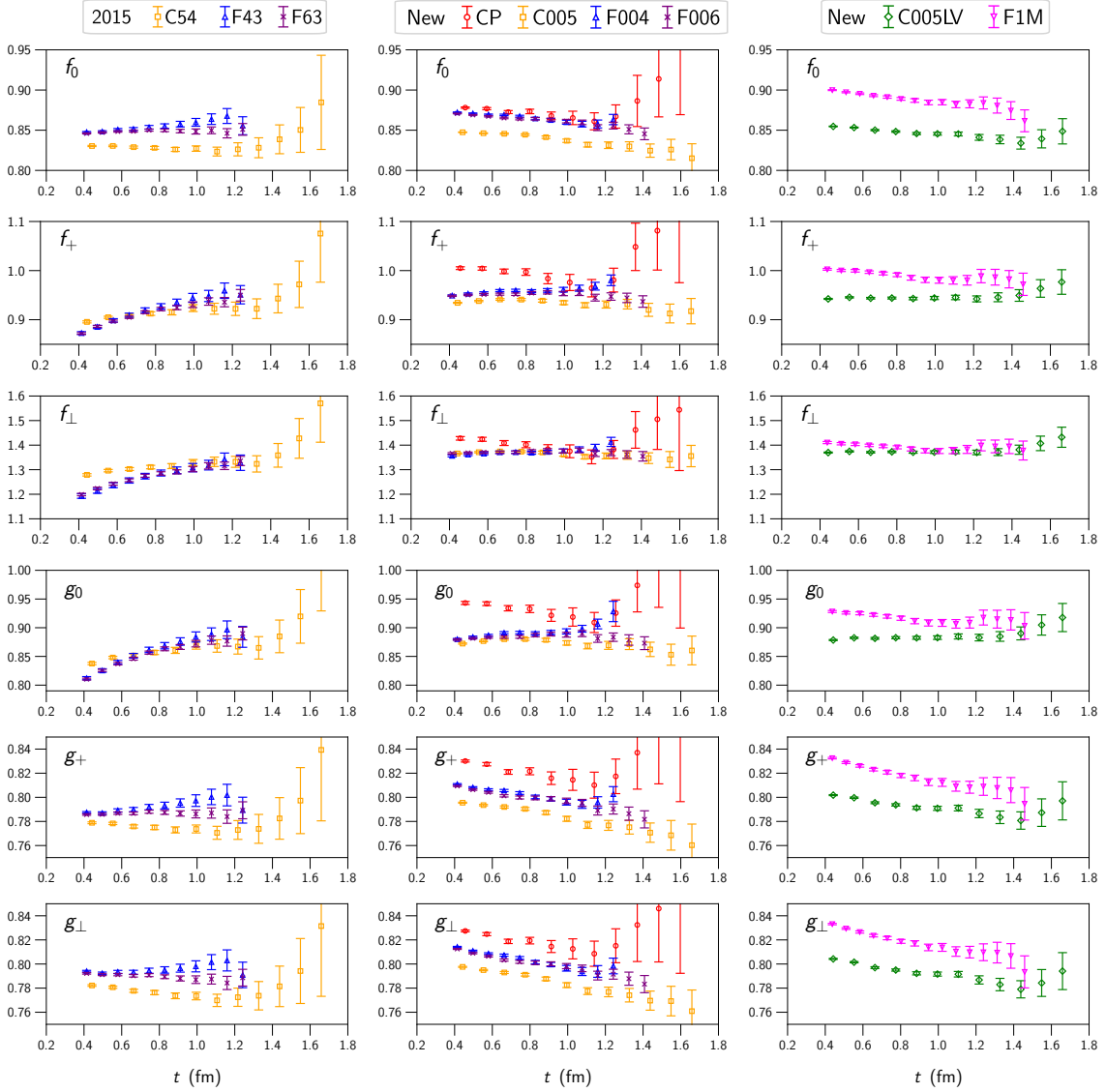


Figure 3: The quantities $R_f(|\mathbf{p}'|, t)$ that, for large t , become equal to the $\Lambda_b \rightarrow \Lambda_c$ vector and axial-vector form factors at $|\mathbf{p}'| \approx 0.8$ GeV. The center and right plots are from the next-generation computations (with preliminary renormalization factors); the left plots show the corresponding 2015 results for comparison.

reason, I only present the results for $R_f(|\mathbf{p}'|, t)$ here, at one kinematic point given by

$$|\mathbf{p}'|^2 = \left\{ \begin{array}{ll} 3 \cdot (2\pi/L)^2 & \text{for C005, F004, F006,} \\ 12 \cdot (2\pi/L)^2 & \text{for CP,} \\ 5 \cdot (2\pi/L)^2 & \text{for C005LV, F1M} \end{array} \right\} \approx (0.8 \text{ GeV})^2. \quad (3)$$

These results are shown in Fig. 3 for $\Lambda_b \rightarrow \Lambda_c$, Fig. 4 for $\Lambda_b \rightarrow \Lambda$, and Fig. 5 for $\Lambda_b \rightarrow p$. The corresponding results from the 2015/2016 data sets with $m_\pi^{(\text{val})} = m_\pi^{(\text{sea})}$ are included for comparison. Note that, at the larger source-sink separations, the fluctuations in the ratio may become too large to compute the square root; such separations are omitted.

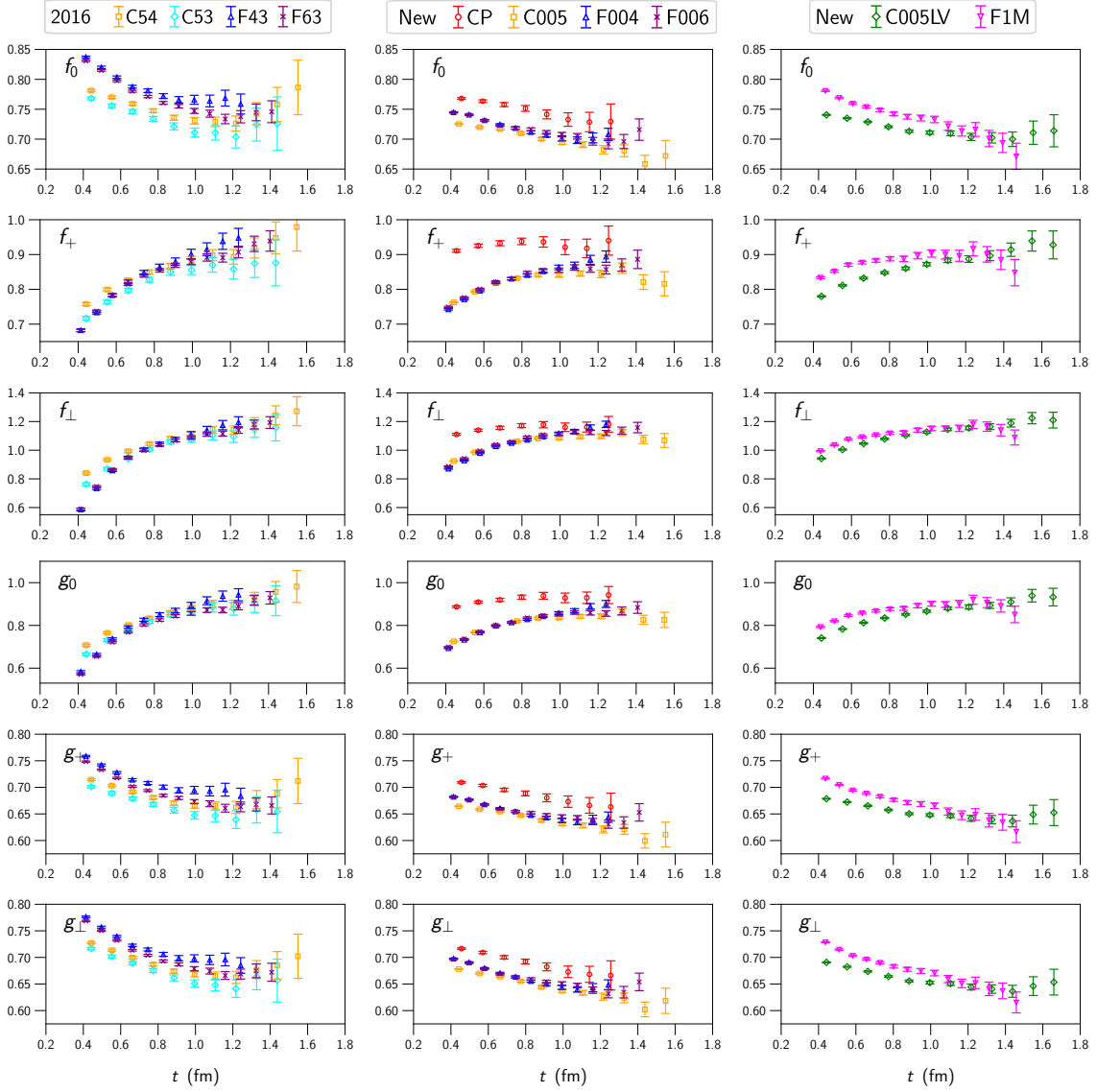
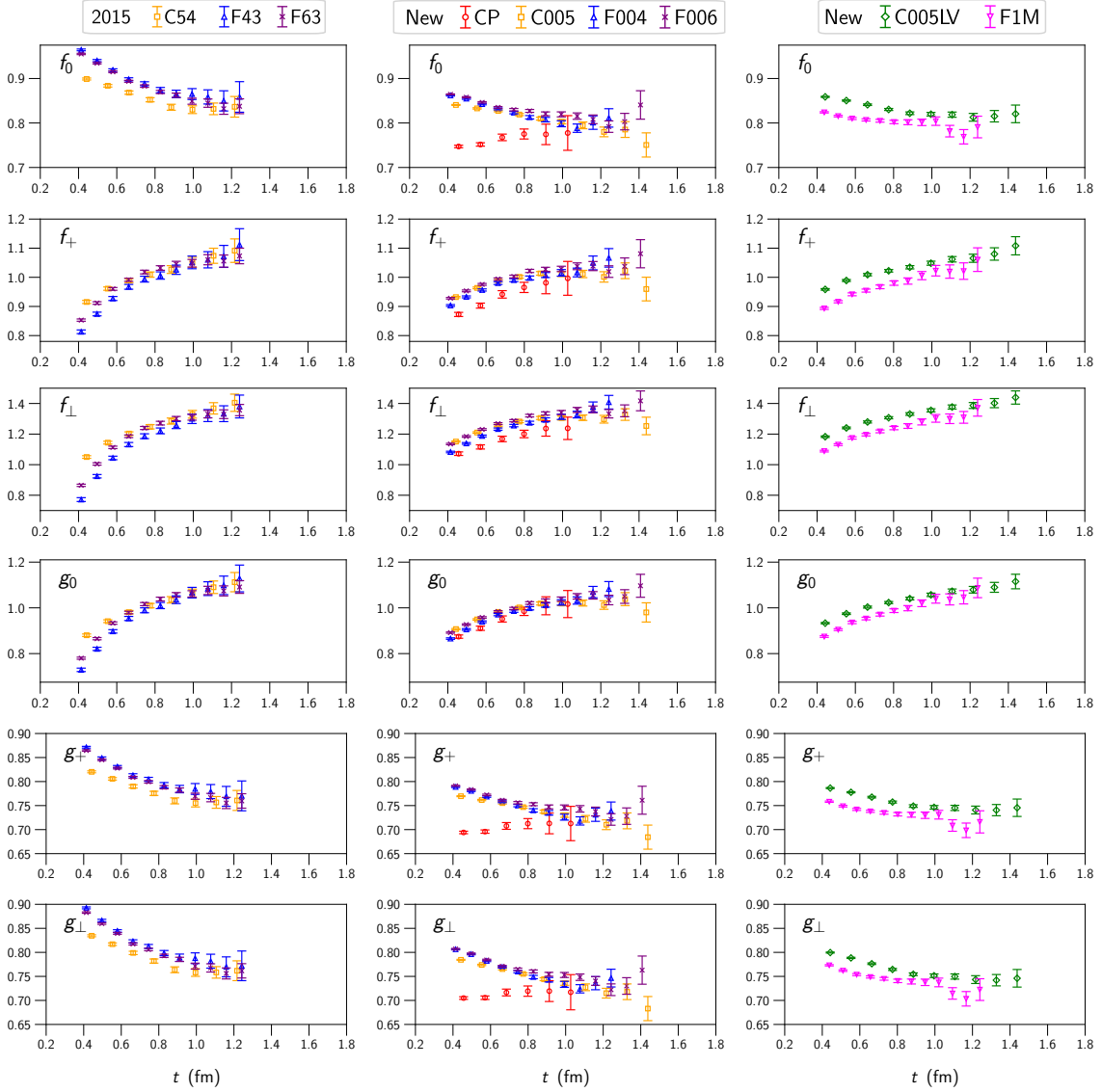


Figure 4: Like Fig. 3, but for $\Lambda_b \rightarrow \Lambda$. In comparing the old and new results, note that the valence strange-quark masses have also changed (see Table 1).

The results for $\Lambda_b \rightarrow \Lambda_c$ have the smallest statistical uncertainties. For some form factors, even after the large- t extrapolation, the dependence on the pion mass and lattice spacing will be clearly resolved with the help of the new CP and F1M data. For $\Lambda_b \rightarrow p$, it appears that the dependence on pion mass and lattice spacing will typically not be significant after extracting the ground-state contributions, in part due to the larger statistical uncertainties. Another feature worth pointing out is that, except for $g_+(\Lambda_b \rightarrow \Lambda_c)$ and $g_\perp(\Lambda_b \rightarrow \Lambda_c)$, the new F004 and F006 data generally show less excited-state contamination (i.e., smaller t -dependence) than the old F43 and F63 data due to the increased smearing width.


Figure 5: Like Fig. 3, but for $\Lambda_b \rightarrow p$.

4. Next steps

The next task is to complete the fits of the t dependence of $R_f(|\mathbf{p}'|, t)$ to extract the ground-state form factors for all data sets and all momenta, after finalizing the values of the residual matching factors ρ_Γ and the $O(a)$ -improvement coefficients in the weak currents. It may also be possible to replace the mostly nonperturbative renormalization method with a fully nonperturbative method [27]. Finally, the chiral/continuum/kinematic extrapolations of the form factors need to be performed. In the kinematic extrapolations, I plan to consider dispersive bounds, whose application to baryon semileptonic form factors using a novel parametrization was discussed in Ref. [28]. The parametrization replaces the usual z^n monomials by polynomials $p_n(z)$ that are orthonormal on the arc of the unit circle that is relevant for the dispersive bounds [29].

Acknowledgments

I thank the RBC and UKQCD collaborations for providing the gauge-field ensembles. I thank Oliver Witzel for sharing preliminary values of the bottom-quark action parameters with me prior to their publication. I am currently supported by the U.S. Department of Energy, Office of Science, Office of High Energy Physics under Award Number DE-SC0009913, and was supported by National Science Foundation Award Number PHY-1520996 and by the RHIC Physics Fellow Program of the RIKEN BNL Research Center during the early stages of this work. I carried out the computations on facilities at the National Energy Research Scientific Computing Center, a DOE Office of Science User Facility supported by the Office of Science of the U.S. Department of Energy under Contract No. DE-AC02-05CH1123, and on facilities of the Extreme Science and Engineering Discovery Environment (XSEDE), which was supported by National Science Foundation grant number ACI-1548562. I used Chroma [30, 31], QLUA [32], MDWF [33], and related USQCD software [34].

References

- [1] **LHCb** Collaboration, R. Aaij *et al.*, “Determination of the quark coupling strength $|V_{ub}|$ using baryonic decays,” *Nature Phys.* **11** (2015) 743–747, [arXiv:1504.01568 \[hep-ex\]](#).
- [2] **LHCb** Collaboration, R. Aaij *et al.*, “Observation of the decay $\Lambda_b^0 \rightarrow \Lambda_c^+ \tau^- \bar{\nu}_\tau$,” *Phys. Rev. Lett.* **128** no. 19, (2022) 191803, [arXiv:2201.03497 \[hep-ex\]](#).
- [3] **LHCb** Collaboration, R. Aaij *et al.*, “Differential branching fraction and angular analysis of $\Lambda_b^0 \rightarrow \Lambda \mu^+ \mu^-$ decays,” *JHEP* **06** (2015) 115, [arXiv:1503.07138 \[hep-ex\]](#). [Erratum: *JHEP* **09**, 145 (2018)].
- [4] **LHCb** Collaboration, R. Aaij *et al.*, “Angular moments of the decay $\Lambda_b^0 \rightarrow \Lambda \mu^+ \mu^-$ at low hadronic recoil,” *JHEP* **09** (2018) 146, [arXiv:1808.00264 \[hep-ex\]](#).
- [5] T. Blake, S. Meinel, and D. van Dyk, “Bayesian Analysis of $b \rightarrow s \mu^+ \mu^-$ Wilson Coefficients using the Full Angular Distribution of $\Lambda_b \rightarrow \Lambda(\rightarrow p \pi^-) \mu^+ \mu^-$ Decays,” *Phys. Rev. D* **101** no. 3, (2020) 035023, [arXiv:1912.05811 \[hep-ph\]](#).
- [6] T. Feldmann and M. W. Y. Yip, “Form factors for $\Lambda_b \rightarrow \Lambda$ transitions in the soft-collinear effective theory,” *Phys. Rev. D* **85** (2012) 014035, [arXiv:1111.1844 \[hep-ph\]](#). [Erratum: *Phys.Rev.D* **86**, 079901 (2012)].
- [7] W. Detmold, C. Lehner, and S. Meinel, “ $\Lambda_b \rightarrow p \ell^- \bar{\nu}_\ell$ and $\Lambda_b \rightarrow \Lambda_c \ell^- \bar{\nu}_\ell$ form factors from lattice QCD with relativistic heavy quarks,” *Phys. Rev. D* **92** no. 3, (2015) 034503, [arXiv:1503.01421 \[hep-lat\]](#).
- [8] W. Detmold and S. Meinel, “ $\Lambda_b \rightarrow \Lambda \ell^+ \ell^-$ form factors, differential branching fraction, and angular observables from lattice QCD with relativistic b quarks,” *Phys. Rev. D* **93** no. 7, (2016) 074501, [arXiv:1602.01399 \[hep-lat\]](#).

- [9] J. Albrecht, F. Bernlochner, M. Kenzie, S. Reichert, D. Straub, and A. Tully, “Future prospects for exploring present day anomalies in flavour physics measurements with Belle II and LHCb,” [arXiv:1709.10308 \[hep-ph\]](#).
- [10] A. Di Canto and S. Meinel, “Weak Decays of b and c Quarks,” [arXiv:2208.05403 \[hep-ex\]](#).
- [11] **RBC/UKQCD** Collaboration, T. Blum *et al.*, “Domain wall QCD with physical quark masses,” *Phys. Rev. D* **93** no. 7, (2016) 074505, [arXiv:1411.7017 \[hep-lat\]](#).
- [12] **RBC/UKQCD** Collaboration, P. A. Boyle, L. Del Debbio, N. Garron, A. Juttner, A. Soni, J. T. Tsang, and O. Witzel, “SU(3)-breaking ratios for $D_{(s)}$ and $B_{(s)}$ mesons,” [arXiv:1812.08791 \[hep-lat\]](#).
- [13] E. Shintani, R. Arthur, T. Blum, T. Izubuchi, C. Jung, and C. Lehner, “Covariant approximation averaging,” *Phys. Rev. D* **91** no. 11, (2015) 114511, [arXiv:1402.0244 \[hep-lat\]](#).
- [14] A. X. El-Khadra, A. S. Kronfeld, and P. B. Mackenzie, “Massive fermions in lattice gauge theory,” *Phys. Rev. D* **55** (1997) 3933–3957, [arXiv:hep-lat/9604004](#).
- [15] P. Chen, “Heavy quarks on anisotropic lattices: The Charmonium spectrum,” *Phys. Rev. D* **64** (2001) 034509, [arXiv:hep-lat/0006019](#).
- [16] S. Aoki, Y. Kuramashi, and S.-i. Tominaga, “Relativistic heavy quarks on the lattice,” *Prog. Theor. Phys.* **109** (2003) 383–413, [arXiv:hep-lat/0107009](#).
- [17] S. Aoki, Y. Kayaba, and Y. Kuramashi, “A Perturbative determination of mass dependent $O(a)$ improvement coefficients in a relativistic heavy quark action,” *Nucl. Phys. B* **697** (2004) 271–301, [arXiv:hep-lat/0309161](#).
- [18] N. H. Christ, M. Li, and H.-W. Lin, “Relativistic Heavy Quark Effective Action,” *Phys. Rev. D* **76** (2007) 074505, [arXiv:hep-lat/0608006](#).
- [19] H.-W. Lin and N. Christ, “Non-perturbatively Determined Relativistic Heavy Quark Action,” *Phys. Rev. D* **76** (2007) 074506, [arXiv:hep-lat/0608005](#).
- [20] **RBC, UKQCD** Collaboration, Y. Aoki, N. H. Christ, J. M. Flynn, T. Izubuchi, C. Lehner, M. Li, H. Peng, A. Soni, R. S. Van de Water, and O. Witzel, “Nonperturbative tuning of an improved relativistic heavy-quark action with application to bottom spectroscopy,” *Phys. Rev. D* **86** (2012) 116003, [arXiv:1206.2554 \[hep-lat\]](#).
- [21] Z. S. Brown, W. Detmold, S. Meinel, and K. Orginos, “Charmed bottom baryon spectroscopy from lattice QCD,” *Phys. Rev. D* **90** no. 9, (2014) 094507, [arXiv:1409.0497 \[hep-lat\]](#).
- [22] **Particle Data Group** Collaboration, R. L. Workman *et al.*, “Review of Particle Physics,” *PTEP* **2022** (2022) 083C01.

- [23] **RBC/UKQCD** Collaboration, J. M. Flynn, R. C. Hill, A. Jüttner, A. Soni, J. T. Tsang, and O. Witzel, “Exclusive semileptonic $B_s \rightarrow K\ell\nu$ decays on the lattice,” *Phys. Rev. D* **107** no. 11, (2023) 114512, [arXiv:2303.11280 \[hep-lat\]](#).
- [24] S. Hashimoto, A. X. El-Khadra, A. S. Kronfeld, P. B. Mackenzie, S. M. Ryan, *et al.*, “Lattice QCD calculation of $\bar{B} \rightarrow D\ell\bar{\nu}$ decay form-factors at zero recoil,” *Phys.Rev.* **D61** (1999) 014502, [arXiv:hep-ph/9906376 \[hep-ph\]](#).
- [25] A. X. El-Khadra, A. S. Kronfeld, P. B. Mackenzie, S. M. Ryan, and J. N. Simone, “The Semileptonic decays $B \rightarrow \pi\ell\nu$ and $D \rightarrow \pi\ell\nu$ from lattice QCD,” *Phys.Rev.* **D64** (2001) 014502, [arXiv:hep-ph/0101023 \[hep-ph\]](#).
- [26] **RBC/UKQCD** Collaboration, P. A. Boyle, L. Del Debbio, A. Jüttner, A. Khamseh, F. Sanfilippo, and J. T. Tsang, “The decay constants f_D and f_{D_s} in the continuum limit of $N_f = 2 + 1$ domain wall lattice QCD,” *JHEP* **12** (2017) 008, [arXiv:1701.02644 \[hep-lat\]](#).
- [27] D. Giusti and C. Lehner, “A new framework to tune an improved relativistic heavy-quark action,” *PoS LATTICE2021* (2022) 042, [arXiv:2111.15614 \[hep-lat\]](#).
- [28] T. Blake, S. Meinel, M. Rahimi, and D. van Dyk, “Dispersive bounds for local form factors in $\Lambda_b \rightarrow \Lambda$ transitions,” [arXiv:2205.06041 \[hep-ph\]](#).
- [29] N. Gubernari, D. van Dyk, and J. Virto, “Non-local matrix elements in $B_{(s)} \rightarrow \{K^{(*)}, \phi\}\ell^+\ell^-$,” *JHEP* **02** (2021) 088, [arXiv:2011.09813 \[hep-ph\]](#).
- [30] **SciDAC, LHPC, UKQCD** Collaboration, R. G. Edwards and B. Joo, “The Chroma software system for lattice QCD,” *Nucl. Phys. B Proc. Suppl.* **140** (2005) 832, [arXiv:hep-lat/0409003](#).
- [31] R. G. Edwards, B. Joó, *et al.*, “Chroma.” <https://github.com/JeffersonLab/chroma>.
- [32] A. Pochinsky, S. Syritsyn, *et al.*, “QLUA.” <https://usqcd.lns.mit.edu/w/index.php/QLUA>.
- [33] A. Pochinsky, S. Syritsyn, *et al.*, “Möbius Domain Wall inverter.” <https://github.com/usqcd-software/mdwf>.
- [34] **USQCD** Collaboration, “USQCD Software.” <http://usqcd-software.github.io>.